Intrinsic stoichiometry and oxygen-induced *p*-type conductivity of pyrite FeS_2

Ruoshi Sun,[1] M. K. Y. Chan,[1,2] ShinYoung Kang (강신영),[1] and G. Ceder[1,*]

[1]*Department of Materials Science and Engineering, Massachusetts Institute of Technology, Cambridge, Massachusetts, USA*

[2]*Center for Nanoscale Materials, Argonne National Laboratory, Argonne, Illinois, USA*

(Received 14 May 2011; published 29 July 2011)

The stoichiometry and ubiquitous observation of *p*-type conductivity of synthetic pyrite FeS_2 thin films are investigated via first-principles computations of native (vacancies, interstitials, antisites) and extrinsic (O_S, O_i) point defects. Native defects have high formation energies and are predicted to occur in low concentrations within the Fe- and S-rich limits, showing that pyrite should be intrinsically stoichiometric. Under sufficiently oxidizing conditions, O_S becomes the most dominant defect type and induces *p*-type conductivity. At the experimental oxygen impurity concentration, the hole concentration is predicted to be $O(10^{19})$ cm^{-3}, in agreement with Hall measurements reported in the literature. Therefore, we attribute the unintentional *p*-type conductivity of pyrite to oxygen impurities and propose that improvements in device performance may be achieved under more reducing conditions.

DOI: 10.1103/PhysRevB.84.035212 PACS number(s): 71.15.Mb, 71.55.−i, 72.40.+w, 61.72.Bb

I. INTRODUCTION

Ever since the first investigation of pyrite FeS_2 as a photovoltaic device,[1] a number of challenges have arisen. We have recently investigated the roles of intrinsic surface states and marcasite.[2] In this paper, we focus on the following two open questions that pertain to native defects and extrinsic impurities. (i) Is pyrite off-stoichiometric or is it a line compound? According to the work of Birkholz *et al.*, pyrite samples are sulfur deficient up to 13 at. %.[3] They have suggested that gap states are introduced by sulfur vacancies, though no experimental or theoretical evidence exists to back up this proposal. By reviewing the literature, Ellmer and Höpfner have argued that the compositional variation of pyrite should be within 1 at. %, and that the 13 at. % S deficiency reported by Birkholz *et al.* is likely to be a measurement error.[4] (ii) Why are synthetic thin films ubiquitously *p* type, regardless of the deposition methods and synthesis conditions, although no intentional doping is performed? (See Ref. 5 and references therein, as well as Refs. 6 and 7.) These issues are important if pyrite is ever to be seriously considered as a photovoltaic material.

It is well known that defects can greatly affect the electronic properties of semiconductor devices.[8] Although experiments have alluded to the presence of bulk defects in pyrite,[9] and computational[10] and combined experimental-computational[11] work have investigated pyrite surface defects, there has been no systematic study of the role of bulk defects within pyrite in the literature. In this paper, we address the stoichiometry (i) and unintentional *p*-type conductivity (ii) of pyrite via first-principles computation and modeling of native and extrinsic defects. Fe and S vacancies, interstitials, and antisites constitute the native defects. For extrinsic defects, we focus on oxygen interstitial (O_i) and oxygen-on-sulfur substitution (O_S), because oxygen has the highest impurity concentration [$O(10^{19})$ cm^{-3}] in both natural and synthetic samples.[12]

In Sec. II we present the input parameters used in our computations as well as a brief review of defect modeling. In Sec. III results for native and oxygen defects are presented, followed by a discussion in Sec. IV. We demonstrate that pyrite is unlikely to be off-stoichiometric due to the high formation energies of its native defects, and that the *p*-type conductivity can be attributed to the high concentration of oxygen incorporation on sulfur sites.

II. METHODS

A. First-principles computations

Density-functional theory (DFT)[13,14] calculations within the Perdew-Burke-Ernzerhof (PBE)[15,16] generalized gradient approximation (GGA) were performed using the plane-wave code Vienna *Ab-initio* Simulation Package (VASP)[17–20] with projector augmented wave (PAW) potentials.[21,22] Total energies were converged to within 10^{-7} eV. Charge neutral point defect formation energies were converged for a supercell size of $2 \times 2 \times 2$ with 95–97 atoms. Charged defect total energies were also obtained from $2 \times 2 \times 2$ supercells. All defective supercells were fully relaxed under constant volume with $3 \times 3 \times 3$ Γ-centered Monkhorst-Pack[23] *k* points. Forces were converged to within 10^{-4} eV/Å.

B. Defect modeling

1. Definitions

We adopt the notation of Persson *et al.*[24] regarding defect computations. Definitions and methodology are briefly summarized as follows. The formation energy of a defect *D* in charge state *q* is

$$\begin{aligned}\Delta H_{D,q}(E_F,\mu_\alpha) &= E_{D,q} - E_0 - \sum_\alpha n_\alpha\left(\mu_\alpha^0 + \Delta\mu_\alpha\right) \\ &\quad + q(E_v + E_F) \\ &= \Delta H_{D,q}^0(\mu_\alpha) + qE_F, \end{aligned} \tag{1}$$

where E_0 is the total energy of the perfect host, α is the atomic species of the defect, μ_α^0 is the reference chemical potential, n_α is the number of atoms introduced into (positive) or removed from (negative) the host, E_v is the eigenvalue of the valence band maximum (VBM), E_F is the Fermi level referenced to the VBM, and $\Delta H_{D,q}^0$ is the defect formation energy at the VBM. We have neglected entropy contributions other than configurational entropy since they usually do not affect results qualitatively.[25]

It is important to note that the E_F in Eq. (1) is merely an energy variable bounded by the position of the band edges. The charge transition level between charge states q and q' of a defect D occurs when their formation energies are the same; that is,

$$\epsilon_{D,q/q'} = \frac{E_{D,q} - E_{D,q'}}{q' - q} - E_v. \tag{2}$$

The E_F in Eq. (1) is replaced with $\epsilon_{D,q/q'}$ in the derivation.

The concentration of a defect in charge state q is given by

$$c_{D,q}(E_F,\mu_\alpha,T) = N_{\text{site}} \exp\left[-\frac{\Delta H_{D,q}(E_F,\mu_\alpha)}{kT}\right], \tag{3}$$

where N_{site} is the concentration of possible defect sites, which is determined by the multiplicity of the defect's Wyckoff position. The total concentration of a certain defect D is obtained by a summation over all the charge states; that is,

$$c_D = \sum_q c_{D,q}. \tag{4}$$

The total charge of the system (Q) is the sum of the defect charge concentration (Q_D) and the free carrier concentrations (Q_i), that is,

$$\begin{aligned} Q(E_F) &= \sum_D \sum_q q c_{D,q}(E_F,\mu_\alpha,T) - n + p \\ &= \sum_D \sum_q q N_{\text{site}} \exp\left[-\frac{\Delta H_{D,q}(E_F,\mu_\alpha)}{kT}\right] \\ &\quad - \int_{E_c}^{\infty} f(E;E_F,T) g(E) dE \\ &\quad + \int_{-\infty}^{E_v} [1 - f(E;E_F,T)] g(E) dE, \end{aligned} \tag{5}$$

where $g(E)$ is the density of states (DOS) of the host, and $Q_i = p - n$ is the hole concentration (p) in the valence band (VB) minus the electron concentration (n) in the conduction band (CB).

The expected charge state q^* of a defect X_Y is defined as the difference in valence between X and Y. For example, the expected charge states of V_{Fe} and V_S are $2-$ and $1+$, respectively. Based on the sign of its expected charge state, a defect can be classified as a donor ($q^* > 0$) or an acceptor ($q^* < 0$).

2. *Self-consistent solution for Fermi level and defect concentrations*

The thermodynamic Fermi level is the E_F at which charge neutrality is satisfied, that is, when $Q = 0$ in Eq. (5). In solving for the defect concentrations and Fermi level we assume that defects are equilibrated at the synthesis temperature (T_{syn}) and are not mobile at room temperature (T_{eq}) due to low diffusion of defects and slow mass exchange with the environment. Only their charge states can reequilibrate at room temperature. Procedural details are as follows.

(i) Impose charge neutrality at T_{syn}; that is,

$$Q_D\left(E_F^{\text{syn}},T_{\text{syn}}\right) + Q_i\left(E_F^{\text{syn}},T_{\text{syn}}\right) = 0. \tag{6}$$

Solving for E_F^{syn}, the concentration of each defect $c_{D,q}$ is found from Eq. (3), and the total concentration of each defect c_D is obtained via Eq. (4).

(ii) We assume that the total concentration of each defect D is frozen during reequilibration at T_{eq}; that is,

$$c_D = c_D\left(E_F^{\text{syn}},T_{\text{syn}}\right) = c_D\left(E_F^{\text{eq}},T_{\text{eq}}\right). \tag{7}$$

Note that individual $c_{D,q}$'s are not fixed since charge transitions can occur even at room temperature.

(iii) Assume charge transition within a defect type D occurs according to Boltzmann statistics. First, observe from Eqs. (1) and (3) that one can always express the ratio between the concentration of D in charge state q and that in some arbitrary reference charge state q' as

$$\frac{c_{D,q}}{c_{D,q'}} = \exp\frac{\Delta H^0_{D,q'} - \Delta H^0_{D,q}}{kT} \exp\frac{(q'-q)E_F}{kT}. \tag{8}$$

We shall denote the prefactor as

$$A_{D,q} = \exp\frac{\Delta H^0_{D,q'} - \Delta H^0_{D,q}}{kT}. \tag{9}$$

By the frozen defect assumption (ii) and using Eq. (4), we then obtain

$$\begin{aligned} c_{D,q}\left(E_F^{\text{eq}},T_{\text{eq}}\right) &= c_D \frac{A_{D,q} \exp\frac{-qE_F^{\text{eq}}}{kT_{\text{eq}}}}{\sum_q A_{D,q} \exp\frac{-qE_F^{\text{eq}}}{kT_{\text{eq}}}} \\ &= c_D \frac{\exp\frac{-\Delta H_{D,q}(E_F^{\text{eq}})}{kT_{\text{eq}}}}{\sum_q \exp\frac{-\Delta H_{D,q}(E_F^{\text{eq}})}{kT_{\text{eq}}}}, \end{aligned} \tag{10}$$

which is independent of the reference charge state q'. The above construct allows us to apportion the total defect concentration c_D obtained at T_{syn} to the concentrations of its different charge states $c_{D,q}$ at T_{eq}.

(iv) For these fixed defect concentrations c_D, charges are reequilibrated at T_{eq}; that is,

$$Q_D\left(E_F^{\text{eq}},T_{\text{eq}}\right) + Q_i\left(E_F^{\text{eq}},T_{\text{eq}}\right) = 0, \tag{11}$$

where

$$Q_D\left(E_F^{\text{eq}},T_{\text{eq}}\right) = \sum_D c_D \frac{\sum_q q \exp\frac{-\Delta H_{D,q}(E_F^{\text{eq}})}{kT_{\text{eq}}}}{\sum_q \exp\frac{-\Delta H_{D,q}(E_F^{\text{eq}})}{kT_{\text{eq}}}}. \tag{12}$$

Thus, having solved for E_F^{eq}, all defect concentrations are fully determined by Eq. (10), while electron and hole concentrations are given by $n(E_F^{\text{eq}},T_{\text{eq}})$ and $p(E_F^{\text{eq}},T_{\text{eq}})$, respectively. We choose $T_{\text{syn}} = 800$ K and $T_{\text{eq}} = 300$ K to simulate experimental conditions.[12]

3. *Reference chemical potentials*

The energies of defects that change the stoichiometry of FeS_2 are determined by the chemical potentials of Fe and S in the environment. It is common to evaluate the off-stoichiometric defects at the limits of chemical potentials

under which the compound is stable. In this work we simply take limits imposed by stability with respect to the elements:

$$\Delta\mu_{\mathrm{Fe}} \leqslant 0, \tag{13}$$

$$\Delta\mu_{\mathrm{S}} \leqslant 0. \tag{14}$$

Together with the relation of the chemical potentials to the energy of the compounds:

$$\Delta\mu_{\mathrm{Fe}} + 2\Delta\mu_{\mathrm{S}} = \Delta H_{\mathrm{FeS_2}}, \tag{15}$$

the Fe-rich/S-poor and S-rich/Fe-poor limits can be defined.

We investigate oxygen incorporation into the material as a function of the oxygen chemical potential referenced to the most reduced iron oxide phase to form from FeS_2, which is Fe_3O_4 based on our computations within GGA. Specifically, we define

$$\mu_{\mathrm{O}}^0 = \tfrac{1}{4}\left(\mu_{\mathrm{Fe_3O_4}} - 3\mu_{\mathrm{Fe}}^0\right) \tag{16}$$

and investigate the Fermi level (E_F^{eq}) and oxygen defect (O_S, O_i) concentrations as a function of $\Delta\mu_{\mathrm{O}} = \mu_{\mathrm{O}} - \mu_{\mathrm{O}}^0$, where a positive (negative) sign corresponds to more oxidizing (reducing) conditions. The total oxygen impurity concentration is given by

$$c_{\mathrm{O}} = \sum_{D\in\{\mathrm{O}_i,\mathrm{O}_S\}} \sum_q c_{D,q}. \tag{17}$$

4. Energy corrections

Three post-DFT corrections are applied. (i) To account for spurious image charge interactions when charged defects are calculated in periodic boundary conditions, we apply the first-order Makov-Payne correction,[26]

$$\Delta E_{D,q}^{\mathrm{MP}} = \frac{q^2\alpha_M}{2\epsilon a_0}, \tag{18}$$

where α_M is the Madelung constant, $\epsilon = 20.6$ is the static dielectric constant we obtain for pyrite using density-functional perturbation theory (DFPT),[27] and a_0 is the GGA lattice constant of pyrite.

(ii) To correct for the underestimated band gap (Kohn-Sham gap $E_g^{\mathrm{KS}} = 0.4$ eV[2] versus experimental gap $E_g^{\mathrm{expt}} = 0.95$ eV[12]), the conduction band minimum (CBM) and VBM of the host DOS are rigidly shifted such that $\Delta E_c - \Delta E_v = \Delta E_g = E_g^{\mathrm{expt}} - E_g^{\mathrm{KS}}$. We determine $\Delta E_v = -0.1$ eV and $\Delta E_c = 0.4$ eV using the Δ-sol method, which is based on screening properties of the perfect host.[28]

(iii) As a result of (ii), donor (acceptor) levels are assumed to move with the CBM (VBM) and thus need to be corrected by the corresponding shift in the band edge; specifically,[24]

$$\Delta E_{D,q}^{g} = \begin{cases} z_e\Delta E_c & \text{if } D \text{ is a donor,} \\ -z_h\Delta E_v & \text{if } D \text{ is an acceptor,} \end{cases} \tag{19}$$

where z_e (z_h) is the number of donor electrons (acceptor holes) in the CB (VB). In terms of the expected charge state of a defect D (defined in Sec. II B 1), $z_e = q^* - q$ and $z_h = q - q^*$. It follows from this procedure that the location of shallow charge transition levels are fixed relative to the appropriate host band edge upon gap correction. (See Ref. 29 for more discussion.) We remark that formation energies of acceptors are adjusted by $q\Delta E_v$ through Eq. (1), in addition to the aforementioned correction. The adjustment applies even when an acceptor D is in its expected charge state q^*, where $z_h = 0$ and $\Delta E_{D,q}^g = 0$.

III. RESULTS

Results on native defects and oxygen incorporation are presented separately. In Sec. III A, formation energies of native defects at Fe- and S-rich limits are examined to address whether pyrite is stoichiometric. In Sec. III B, the role of oxygen point defects are investigated to explain the unintentional p-type conductivity of as-deposited pyrite thin films.

A. Native defects

The defect formation energy at the Fe-rich limit is plotted as a function of E_F in Fig. 1. For each defect, the concave lower envelope of the formation energies for each charge state is drawn to show the lowest-energy charge state along its position within the band gap. The slope of $\Delta H_{D,q}$ is the charge state of D from Eq. (1). Charge transition levels occur at the intersections between different q's, as governed by Eq. (2). The minimum and maximum energies on the x axis correspond to the VBM and the CBM, respectively. The band gap is corrected to match the experimental gap 0.95 eV, as mentioned in Sec. II B 4. Near the VB, the lowest-energy defects are Fe_i and V_S, both carrying positive charges. The concept of defect compensation can be illustrated by the following thought experiment. Suppose E_F^{eq} is drawn toward the VB by some extrinsic acceptor X, then p-type doping becomes increasingly difficult as compensating defects (+) become more and more energetically favorable. Whether a doping limitation is present depends on the actual formation energy of the extrinsic acceptor relative to the minimum formation energy of native compensating defects, which is ~2.5 eV in this case. If the acceptor formation energy is much less than 2.5 eV, then $c_{X,-}$ becomes the dominating term in Eq. (5), and the Fermi level is expected to shift greatly toward

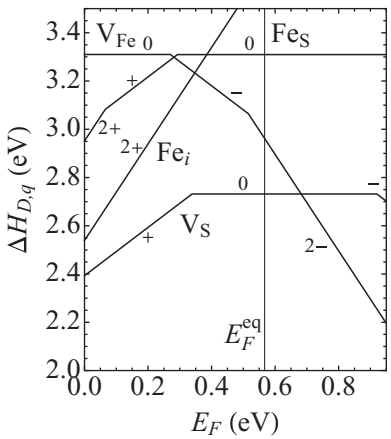

FIG. 1. Defect formation energy as a function of E_F at the Fe-rich limit, where $E_F^{\mathrm{eq}} = 0.57$ eV.

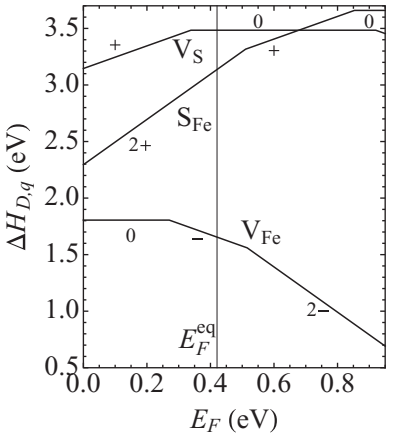

FIG. 2. Defect formation energy as a function of E_F at the S-rich limit, where $E_F^{eq} = 0.42$ eV.

the VB to generate a comparable hole concentration p. In that case, no p-doping limitation would be expected. Likewise, near the CB, the lowest-energy defect is V_{Fe}, whose formation energy is 2.2 eV at the CBM. This suggests that a limitation on n-doping should be about equally unlikely as that on p-doping. We return to this point in Sec. IV.

Following the procedure delineated in Sec. II B 2, a unique solution E_F^{eq} is found within the gap and marked as a vertical line. Here $E_F^{eq} = 0.57$ eV, which is larger than $E_g/2$ due to the asymmetry of the DOS at the band edges. [A flat tail is found at the CBM but not the VBM; there are more states at the VBM than the CBM (see Ref. 2).] The dominant defects are V_S and Fe_S, with concentrations of $O(10^6)$ cm^{-3}. The equilibrium carrier concentrations in the VB and CB are 1.9×10^{12} cm^{-3} for both holes and electrons, respectively, indicating intrinsic behavior. From Eq. (5), since $c_{D,q} \ll n, p$ for all D, the charge neutrality criterion simply becomes $n \approx p$, explaining the intrinsic nature of the material. Since defect concentrations are at most $O(10^6)$ cm^{-3}, pyrite is essentially stoichiometric under these chemical conditions.

At the S-rich limit (Fig. 2), the lowest-energy defect is V_{Fe}, with a total concentration of 5.4×10^{14} cm^{-3}. The defect formation energy of V_S is about 0.8 eV higher than that in the Fe-rich limit, resulting in negligible concentrations. Compared to V_{Fe}, the formation energies of all other defects in the S-rich limit are at least 1 eV larger; thus, they do not play an important role.

The degree of off-stoichiometry of pyrite, or any compound, can be directly predicted by the equilibrium concentration of its native defects. In principle, the off-stoichiometry should be calculated at the chemical potential reference corresponding to experimental conditions. Although the exact reference is unknown, the defect energetics and hence the physics of the system are bounded between the Fe-rich and the S-rich limits. By inspection of Eq. (1), defect formation energies at any allowable chemical potential reference can be obtained by linear interpolation between the two limits. From our results as presented above, the concentration of off-stoichiometric defects is at most on the order of 10^{14} cm^{-3}. Moreover, we believe that reference chemical potentials at experimental conditions should lean toward the Fe-rich limit for the following reasons. (i) The unresolved issue is whether pyrite is S deficient,[3,4] which is more likely to occur under Fe-rich conditions than S-rich conditions. (ii) Fe deficiency due to V_{Fe} has not been reported, implying the environment is Fe rich. (iii) A common method employed to synthesize pyrite is the sulfurization of Fe metal,[30] which corresponds to the Fe-rich limit. At the Fe-rich limit, defect concentrations are merely $O(10^6)$ cm^{-3}. Therefore, pyrite should be stoichiometric when pure. Even at the S-rich limit, it would remain essentially stoichiometric, where an Fe deficiency of 10^{-8} per formula unit is predicted.

B. Oxygen as an acceptor

Oxygen is a common species in the environment and often present in many materials, even if the composition would not indicate so. For example, it forms a detrimental deep state in AlGaN (Ref. 25) and occurs in high concentrations in both as-deposited Si (Ref. 31) and FeS_2 (Ref. 12). We have investigated the possibility of oxygen incorporation into pyrite under reasonable oxidation conditions by calculating the formation energies of the oxygen-on-sulfur substitutional point defect (O_S) and oxygen interstitial (O_i). Using these energies, and together with the formation energies of native defects as calculated in Sec. III A, we solve for the Fermi level and defect concentrations by the same procedure in Sec. II B 2 across a range of $\Delta\mu_O$ as defined in Sec. II B 3. Results at the Fe-rich limit, for reasons discussed at the end of Sec. III A, are presented. Note that, at the S-rich limit, μ_O^0 can be higher [Eq. (16)].

In Fig. 3 the Fermi level is plotted as a function of $\Delta\mu_O$. The bottom-most and topmost energies on the y axis correspond to the VBM and CBM, respectively. Under highly reducing conditions at $T_{syn} = 800$ K, the equilibrium Fermi level remains at the intrinsic level (0.57 eV in Fig. 1). At higher oxidation environments and higher temperature the Fermi level moves toward the VB. A Fermi level below (above) the intrinsic 0.57-eV value indicates that the system is p type (n type). Clearly, under more oxidizing conditions, pyrite becomes increasingly p type.

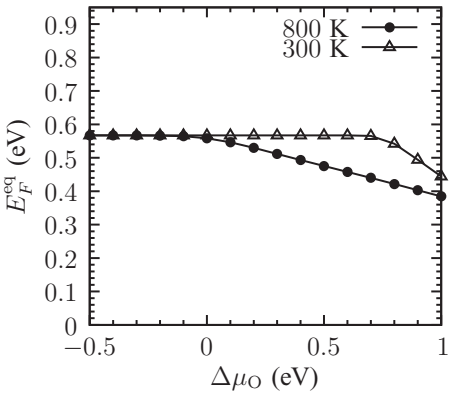

FIG. 3. Equilibrium Fermi level as a function of $\Delta\mu_O$ under $T_{syn} = 800$ K (solid circles) and $T_{syn} = 300$ K (open triangles). Pyrite becomes increasingly p type as the environment becomes more oxidizing.

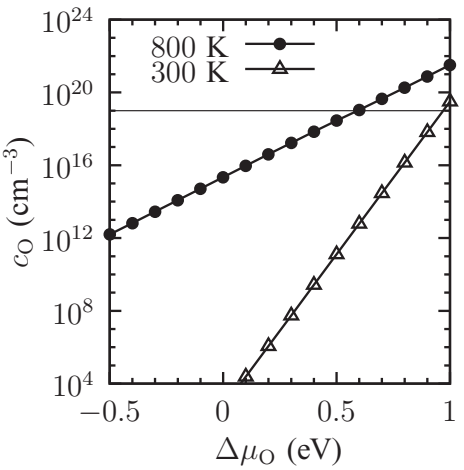

FIG. 4. Oxygen impurity concentration [c_O defined in Eq. (17)] as a function of $\Delta\mu_O$ under $T_{syn} = 800$ K (solid circles) and $T_{syn} = 300$ K (open triangles). The experimental concentration (10^{19} cm^{-3}, horizontal line) corresponds to $\Delta\mu_O = 0.6$ eV at 800 K. The concentration of oxygen impurities increases exponentially as the environment becomes more oxidizing. For $\Delta\mu_O > 1$ eV, essentially all sulfur sites are occupied by oxygen.

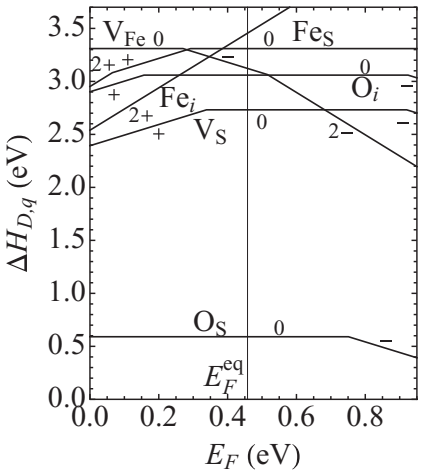

FIG. 5. Defect formation energy as a function of E_F at the Fe-rich limit and $\Delta\mu_O = 0.6$ eV, where $E_F^{eq} = 0.46$ eV. Formation energy lines of native defects are identical to those in Fig. 1.

The corresponding total oxygen impurity concentration is shown in Fig. 4. The parts-per-billion (ppb) and parts-per-million (ppm) oxygen concentrations correspond to $\Delta\mu_O$'s of about -0.3 and 0.1 eV, respectively. For $\mu_O < -0.5$ eV, oxygen incorporation is negligible compared to native defect concentrations. The exponential increase in c_O as a function of $\Delta\mu_O$ is expected by inspection of Eqs. (1) and (3). For $\Delta\mu_O > 1$ eV, all sulfur atoms in pyrite are essentially substituted by oxygen. We find that the experimental oxygen concentration ($\sim 10^{19}$ cm^{-3}) is reached for $\Delta\mu_O \approx 0.6$ eV. The system is examined in detail at this oxygen chemical potential.

In Fig. 5 we show the defect formation energies at $\Delta\mu_O = 0.6$ eV. Since the oxygen chemical potential does not enter into the charge transition levels of native defects [Eq. (2)], the ΔH lines of native defects are not affected by the presence of oxygen. While O_i is highly unfavorable (formation energy 3.1 eV), O_S is the most energetically favorable defect within the system. The Fermi level is pulled down from the intrinsic value 0.57 to 0.46 eV. Although the change in the Fermi level induced by oxygen alters $\Delta H_{D,q}(E_F^{eq})$ for native defects, their energies are still too high compared with ΔH_{O_S} (Table I). Hence, the lowering of the Fermi level is solely caused by O_S.

In Figs. 3 and 4 we also compute the Fermi level and oxygen concentration at $T_{syn} = 300$ K. The Fermi level is not perturbed until $\Delta\mu_O \approx 0.7$ eV. The onset of the Fermi level drop at both temperatures in Fig. 3 corresponds to the same $c_O \approx 10^{15}$ cm^{-3} in Fig. 4.

IV. DISCUSSION

Within the Fe- and S-rich limits, concentrations of native defects are low due to their high formation energies. Intrinsically, pure pyrite is expected to be stoichiometric. Off-stoichiometric experimental samples may be attributed to the presence of other phases with lower S content, for example, pyrrhotite $Fe_{1-x}S$. Ellmer and Höpfner[4] have calculated the formation energies of S and Fe vacancies using the macroscopic cavity model.[32] Although their energies are systematically lower (1.66 and 2.18 eV, respectively)[4] than our calculations (2.73 and 2.96 eV, respectively), we agree qualitatively that these native defects are energetically unfavorable and do not cause noticeable off-stoichiometry in FeS_2. Our study provides a first-principles basis for the high formation energy of native defects within the material.

From Fig. 2 intrinsic p-type conductivity of pyrite is predicted at the S-rich limit. The most energetically favorable defect is V_{Fe}^-, with a concentration of 5.2×10^{14} cm^{-3}. The hole concentration is almost the same (5.5×10^{14} cm^{-3}), as expected by Eq. (11). However, since the experimental

TABLE I. Defect formation energies and concentrations of O_S under Fe-rich environment and $\Delta\mu_O = 0.6$ eV. It can be verified that $\sum_q c_{D,q}(E_F^{eq}) = \sum_q c_{D,q}(E_F^{syn})$, as required by the frozen defect assumption in Sec. II B 2. Energies (concentrations) of other defects are too high (low) and are not shown.

q	$\Delta H^0_{D,q}$ (eV)	$\Delta H_{D,q}\left(E_F^{eq}\right)$ (eV)	$c_{D,q}\left(E_F^{syn}\right)$ (cm^{-3})	$c_{D,q}\left(E_F^{eq}\right)$ (cm^{-3})
2+	1.19	2.10	2.82×10^{7}	4.49×10^{-7}
1+	0.78	1.24	8.08×10^{13}	1.54×10^{8}
0	0.59	0.59	9.65×10^{18}	1.10×10^{19}
1−	1.34	0.88	1.39×10^{18}	1.30×10^{14}
2−	2.42	1.51	1.67×10^{15}	4.42×10^{3}

condition is expected to be Fe-rich, as discussed in Sec. III A, the p-type conductivity should not be attributed to the Fe vacancy. Because oxygen is experimentally measured to have the highest impurity concentration in both synthetic and natural samples,[12] we have examined the role of oxygen impurities.

The experimental oxygen impurity concentration, $O(10^{19})$ cm^{-3}, is reached when $\Delta\mu_O = 0.6$ eV. From Table I, the most dominant defects are O_S^0 (1.1×10^{19} cm^{-3}) and O_S^- (1.30×10^{14} cm^{-3}). Since the oxidation state of S is -1 in pyrite,[33] O_S is expected to be an acceptor with charge state $q^* = 1-$. The prevalence of the charge-neutral defect is very unusual, which at first sight may suggest the formation of an anomalous peroxysulfide bond $[O–S]^{2-}$. To investigate the nature of O_S^0, we show in Fig. 6 the charge density difference between the supercell with a charge-neutral O_S defect and the perfect host, with an isosurface of ± 0.0155 e/Å^3. Negative charge is drawn to O from the neighboring S and Fe atoms. Thus, the oxygen defect is stabilized by partial oxidation of its nearest neighbors, and there is no anomalous bond formation. Likewise, we have also examined the charge density difference between supercells with O_S^0 and O_S^- defects (not shown). There is no difference observed around the O_S defect. Instead, negative charge is attracted to each of the neighboring Fe atoms. Hence, the Fe_n–O_S defect complex is essentially an O^{2-} on a S site with charge state variability accommodated on the neighboring Fe atoms. By Table I and Eq. (11), then, an effective hole carrier concentration of 1.1×10^{19} cm^{-3} is predicted. From experimental Hall measurements of pyrite (without intentional doping) conducted by Willeke *et al.*, the hole concentration is 5×10^{18} cm^{-3} (Ref. 35). The remarkable agreement in the hole concentration between our calculation and experiment, together with the high oxygen impurity concentration,[12] gives strong evidence that the p-type conductivity of pyrite is oxygen-induced.

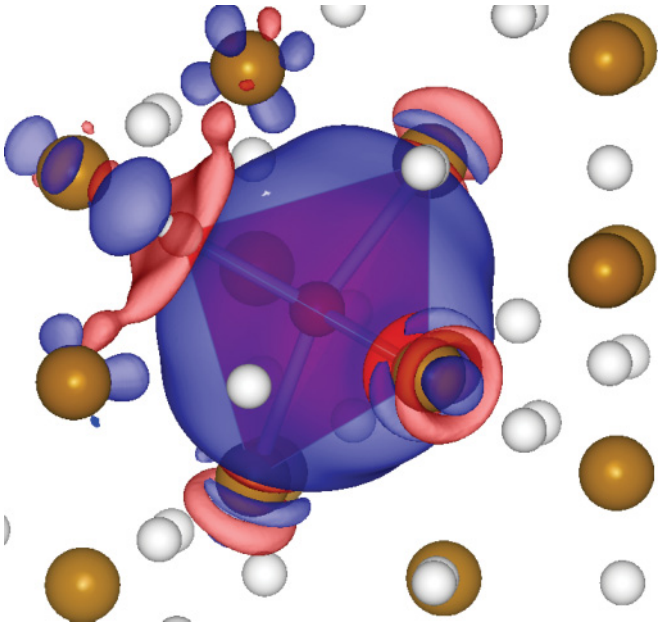

FIG. 6. (Color online) Charge density difference (rendered by VESTA[34]) between a supercell with an O_S^0 defect and the perfect FeS_2 host, viewed in the (111) plane. Positive and negative 0.0155 e/Å^3 isosurfaces are drawn in red and blue, respectively. The O atom (dark red) is located within a tetrahedral environment of one S (gray) atom and three Fe (brown) atoms. The charge state of O_S is effectively $1-$ due to charge transfer from its nearest neighbors, as discussed in the text.

We draw an analogy between this work and Van de Walle and Neugebauer's work on AlGaN, in which they show that unintentional n-type conductivity is not caused by V_N, as its formation energy is too high, but is caused by oxygen contamination.[25] While the substitutional O atom in AlGaN causes significant lattice relaxation around the impurity,[36] it is essentially located at the S site in pyrite. The presence of O_S may undermine device performance by serving as a Shockley-Read-Hall recombination center. Indeed, since the 0 and $1-$ charge states are the most energetically favorable defects within the system, the O_S defect can trap both mobile electrons and holes:

$$O_S^0 + e^- \rightarrow O_S^-, \tag{20}$$

$$O_S^- + h^+ \rightarrow O_S^0. \tag{21}$$

In the electron trapping mechanism [Eq. (20)], the electron is not trapped by the O atom, but by its partially oxidized nearest neighbors within the Fe_n–O_S defect complex, as discussed earlier.

It is clear from Figs. 3 and 4 that oxygen incorporation can be reduced by either lowering the temperature or synthesizing under more reducing environments. For example, to reduce c_O to 1 ppm ($\sim 10^{16}$ cm^{-3}) at $T_{syn} = 800$ K, $\Delta\mu_O$ should be decreased to 0.1 eV. Since

$$\delta\Delta\mu_O = kT_{syn} \ln \frac{p_{O_2}}{p_{O_2}^0}, \tag{22}$$

the oxygen partial pressure must be reduced by a factor of 1000 with respect to existing experimental conditions. In the case of as-deposited Si, O contamination occurs on the order of 10^{19}–10^{21} cm^{-3}, causing unwanted n-type behavior.[31] Torres *et al.* have shown that even a mere reduction of oxygen incorporation by 2 orders of magnitude improves device performance.[31] We believe that the performance of pyrite photovoltaic devices can be similarly enhanced by lowering the concentration of oxygen impurities.

Returning to the dopability implication in Sec. III A, we do not expect any n- or p-doping limitations. The formation energies of native defects lie well above 0 in all allowable chemical potential and Fermi level ranges (Figs. 1 and 2), negating the possibility of Fermi level pinning by native defects. [Fermi level pinning is the position of the Fermi level at which the formation energy of a compensating defect becomes 0 (Ref. 24)]. Indeed, pyrite can be doped n-type by elements such as Co (Refs. 5 and 37) and Ni (Ref. 37) with carrier concentrations as high as 10^{20} cm^{-3} (Ref. 5); intentional p-type doping by P has also been achieved.[38] Since device measurements are made on pyrite photoelectrochemical cells instead of p-n junctions,[12] poor performance cannot be attributed to a limited dopability. The more plausible bottleneck is oxygen contamination, which not only behaves as a trap for mobile carriers, but also explains the ubiquitous observation of unintentional p-type conductivity. Future experiments that seek to improve device performance may investigate along these lines.

V. CONCLUSIONS

On the basis of the first-principles modeling of the point defects in pyrite presented in this work, we find that native defects have high formation energies, and that their equilibrium concentrations are too low for pure pyrite to be off-stoichiometric. The presence of oxygen impurities leads to a drop in the Fermi level toward the VB. This unintentional p-type doping effect is more prominent as the environment becomes more oxidizing. At higher temperatures, the onset of such an effect occurs under more reducing conditions. At the experimental oxygen impurity concentration, we predict a hole concentration of $O(10^{19})$ cm^{-3}, in agreement with experimental Hall measurements.[35] Therefore, the unintentional p-type conductivity of synthetic pyrite thin films can be explained via the presence of O_S, which may act as a Shockley-Read-Hall recombination center. To improve device performance, the current parts-per-thousand oxygen impurity concentration[12] must be significantly reduced.

VI. ACKNOWLEDGMENTS

R.S., M.K.Y.C., and S.Y.K. were partially funded by the Chesonis Family Foundation under the Solar Revolution Project. R.S. was also funded by the Department of Energy under Contract No. DE-FG02-96ER45571. This research was supported in part by the National Science Foundation through TeraGrid resources provided by Texas Advanced Computing Center under Grant No. TG-DMR970008S.

*gceder@mit.edu

[1] W. Jaegermann and H. Tributsch, J. Appl. Electrochem. **13**, 743 (1983).
[2] R. Sun, M. K. Y. Chan, and G. Ceder, Phys. Rev. B **83**, 235311 (2011).
[3] M. Birkholz, S. Fiechter, A. Hartmann, and H. Tributsch, Phys. Rev. B **43**, 11926 (1991).
[4] K. Ellmer and C. Höpfner, Philos. Mag. A **75**, 1129 (1997).
[5] J. Oertel, K. Ellmer, W. Bohne, J. Röhrich, and H. Tributsch, J. Cryst. Growth **198**, 1205 (1999).
[6] S. Bausch, B. Sailer, H. Keppner, G. Willeke, E. Bucher, and G. Frommeyer, Appl. Phys. Lett. **57**, 25 (1990).
[7] G. Smestad, A. Ennaoui, S. Fiechter, H. Tributsch, W. K. Hofmann, M. Birkholz, and W. Kautek, Sol. Energy Mater. **20**, 149 (1990).
[8] S. T. Pantelides, Rev. Mod. Phys. **50**, 797 (1978).
[9] M. Bronold, C. Pettenkofer, and W. Jaegermann, J. Appl. Phys. **76**, 5800 (1994).
[10] A. Stirling, M. Bernasconi, and M. Parrinello, Phys. Rev. B **75**, 165406 (2007).
[11] K. Andersson, M. Nyberg, H. Ogasawara, D. Nordlund, T. Kendelewicz, C. S. Doyle, G. E. Brown, L. G. M. Pettersson, and A. Nilsson, Phys. Rev. B **70**, 195404 (2004).
[12] A. Ennaoui, S. Fiechter, C. Pettenkofer, N. Alonso-Vante, K. Büker, M. Bronold, C. Höpfner, and H. Tributsch, Sol. Energy Mater. Sol. Cells **29**, 289 (1993).
[13] P. Hohenberg and W. Kohn, Phys. Rev. **136**, 864 (1964).
[14] W. Kohn and L. J. Sham, Phys. Rev. **140**, 1133 (1965).
[15] J. P. Perdew, K. Burke, and M. Ernzerhof, Phys. Rev. Lett. **77**, 3865 (1996).
[16] J. P. Perdew, K. Burke, and M. Ernzerhof, Phys. Rev. Lett. **78**, 1396 (1997).
[17] G. Kresse and J. Hafner, Phys. Rev. B **47**, 558 (1993).
[18] G. Kresse and J. Hafner, Phys. Rev. B **49**, 14251 (1994).
[19] G. Kresse and J. Furthmüller, Phys. Rev. B **54**, 11169 (1996).
[20] G. Kresse and J. Furthmüller, Comput. Mater. Sci. **6**, 15 (1996).
[21] P. E. Blöchl, Phys. Rev. B **50**, 17953 (1994).
[22] G. Kresse and D. Joubert, Phys. Rev. B **59**, 1758 (1999).
[23] H. J. Monkhorst and J. D. Pack, Phys. Rev. B **13**, 5188 (1976).
[24] C. Persson, Y.-J. Zhao, S. Lany, and A. Zunger, Phys. Rev. B **72**, 035211 (2005).
[25] C. G. Van de Walle and J. Neugebauer, J. Appl. Phys. **95**, 3851 (2004).
[26] G. Makov and M. C. Payne, Phys. Rev. B **51**, 4014 (1995).
[27] M. Gajdoš, K. Hummer, G. Kresse, J. Furthmüller, and F. Bechstedt, Phys. Rev. B **73**, 045112 (2006).
[28] M. K. Y. Chan and G. Ceder, Phys. Rev. Lett. **105**, 196403 (2010).
[29] S. Lany and A. Zunger, Phys. Rev. B **78**, 235104 (2008).
[30] I. Ferrer, D. Nevskaia, C. de las Heras, and C. Sanchez, Solid State Commun. **74**, 913 (1990).
[31] P. Torres, J. Meier, R. Fluckiger, U. Kroll, J. A. A. Selvan, H. Keppner, A. Shah, S. D. Littelwood, I. E. Kelly, and P. Giannoules, Appl. Phys. Lett. **69**, 1373 (1996).
[32] J. C. Phillips and J. A. Van Vechten, Phys. Rev. Lett. **30**, 220 (1973).
[33] S. Harmer and H. Nesbitt, Surf. Sci. **564**, 38 (2004).
[34] K. Momma and F. Izumi, J. Appl. Crystallogr. **41**, 653 (2008).
[35] G. Willeke, R. Dasbach, B. Sailer, and E. Bucher, Thin Solid Films **213**, 271 (1992).
[36] C. G. Van de Walle, Phys. Rev. B **57**, R2033 (1998).
[37] S. Lehner, K. Savage, and J. Ayers, J. Cryst. Growth **286**, 306 (2006).
[38] O. Blenk, E. Bucher, and G. Willeke, Appl. Phys. Lett. **62**, 2093 (1993).